Catalysis Science & Technology

Reforming of methane with carbon dioxide over cerium oxide promoted nickel nanoparticles deposited on 4-channel hollow fibers by atomic layer deposition

Journal:	*Catalysis Science & Technology*
Manuscript ID	CY-ART-01-2020-000039.R1
Article Type:	Paper
Date Submitted by the Author:	22-Feb-2020
Complete List of Authors:	Jin, Baitang; Missouri University of Science and Technology, Department of Chemical and Biochemical Engineering Shang, Zeyu; Missouri University of Science and Technology, Chemical and Biochemical Engineering Li, Shiguang; Gas Technology Institute, Jiang, Yingbing; University of New Mexico, E & PS; Center for Micro Engineered Materials Gu, Xuehong; Nanjing Tech University, Liang, Xinhua; Missouri University of Science and Technology, Chemical and Biochemical Engineering

Reforming of methane with carbon dioxide over cerium oxide promoted nickel nanoparticles deposited on 4-channel hollow fibers by atomic layer deposition

Baitang Jin[a], Zeyu Shang[a], Shiguang Li[b], Ying-Bing Jiang[c], Xuehong Gu[d], and Xinhua Liang[a,*]

[a] *Department of Chemical and Biochemical Engineering, Missouri University of Science and Technology, Rolla, Missouri 65409, United States*

[b] *Gas Technology Institute, 1700 South Mount Prospect Road, Des Plaines, Illinois 60018, United States*

[c] *TEM Laboratory, University of New Mexico, Albuquerque, New Mexico 87131, United States*

[d] *State Key Laboratory of Materials-Oriented Chemical Engineering, College of Chemistry and Chemical Engineering, Nanjing Tech University, 5 Xinmofan Road, Nanjing 210009, P.R. China*

* Corresponding author. Email: liangxin@mst.edu

Abstract

Ni nanoparticles were deposited on four-channel structured α-Al_2O_3 hollow fibers by atomic layer deposition (ALD). CeO_2 was loaded by a liquid phase incipient wetness method to promote Ni catalysts for dry reforming of methane. For Ni/Al_2O_3 prepared by ALD, inactive $NiAl_2O_4$ that originated from the Ni ALD process was incompletely reduced. The introduced CeO_2 was found to weaken the NiO-Al_2O_3 interaction, free NiO from NiO-Al_2O_3 or $NiAl_2O_4$, and improve the reducibility of NiO. The higher reducibility of $NiAl_2O_4$, tuned by CeO_2, further activated the catalyst during DRM, because a larger proportion of $NiAl_2O_4$ was gradually reduced to metallic nickel by the reaction products. The optimal catalytic performance reached a methane reforming

rate of 2,410 $Lh^{-1}g_{Ni}^{-1}$ at 850 °C. The CeO_2 promoted catalyst also exhibited an excellent performance after regeneration. In addition, the inhibition effect of CeO_2 on coke formation was observed, due to the enhanced CO_2 dissociative adsorption by CeO_2.

Keywords: dry reforming of methane; CeO_2; metal-support interaction; atomic layer deposition (ALD)

1. Introduction

Recently, considerable attention has been paid to the catalytic process of dry reforming of methane (DRM), converting greenhouse gases (e.g., methane and carbon dioxide) into valuable syngas (i.e., carbon monoxide and hydrogen). Via chemical recycling of CO_2, this DRM reaction exhibits a significant environmental impact on the utilization of CO_2 or CO_2-rich natural gas and the control of greenhouse gas emission. In addition, the H_2/CO molar ratio of the generated syngas is less than 1, due to the accompanying reverse water-gas shift reaction, which is beneficial in producing valuable C_{5+} liquid hydrocarbons via Fischer-Tropsch synthesis (FTS).[1, 2] Different metal-based catalysts, such as noble metals (e.g., Rh,[3] Pt,[4] Pd,[5] and Ru[6]) and Ni[7] catalysts, have been studied for DRM reactions. Considering economics and catalytic activity, nickel-based catalysts are the most widely investigated catalysts in the methane reforming field. However, the proneness to sintering and coking at high temperatures remain as a challenge.[8, 9]

In terms of nickel-based catalysts, Al_2O_3 is the most commonly used support. The metal-support interaction of the Ni/Al_2O_3 catalyst plays an important role, as the nickel atoms may diffuse into Al_2O_3 to some extent,[10] depending on factors, such as nickel loading,[11] synthesis parameters,[10, 12-

[14] temperature of heat treatment,[15] and promoters.[16] For example, Zhou et al. prepared a $Ni/NiAl_2O_4/Al_2O_3$/alloy catalyst for steam reforming of methane and found the interfacial $NiAl_2O_4$ layer could anchor the metallic nickel nanoparticles and effectively suppress sintering.[13] In our previous work,[12] $Ni/\gamma\text{-}Al_2O_3$ catalysts were prepared by the atomic layer deposition (ALD) method and they exhibited a stronger $NiO\text{-}Al_2O_3$ interaction than that of catalysts prepared by the conventional incipient wetness (IW) method. The $NiAl_2O_4$ spinel is important for stabilizing metallic nickel nanoparticles, although it has no intrinsic activity for the DRM reaction.[15, 17] Jiménez-González et al. successfully synthesized nickel catalysts with high dispersion and small size by reducing $NiAl_2O_4$ or $NiAl_2O_4/Al_2O_3$ at high temperatures.[18] Recently, our group found that the mixture of H_2 and CO, as a product of DRM, could gradually reduce $NiAl_2O_4$ to Ni at 850 ˚C.[12] The gradual reduction of $NiAl_2O_4$, during the DRM reaction, resulted in an activation phenomenon and, thereby, a higher activity.[12, 17, 19, 20] Since there was a significant amount of $NiAl_2O_4$ component in the Ni/Al_2O_3 catalysts prepared by ALD, and this $NiAl_2O_4$ component cannot be completely reduced but remains inactive in the catalyst, it would be important to tune the reducibility of $NiAl_2O_4$ to generate more metallic Ni to have a higher catalytic activity.

Adding promotors (e.g., Co,[21] ZrO_2,[22] CeO_2,[23] MgO,[24] and CaO[25]) to nickel-based catalysts is an effective and conceivable way to promote the Ni/Al_2O_3 catalysts. CeO_2 could modify the metal-support interaction of Ni catalysts, which could improve the reducibility of Ni/Al_2O_3 catalysts.[16, 26-28] In addition, CeO_2 contains a high concentration of highly mobile oxygen that acts as an oxygen source for the reactions carried out on its surface,[23] which is helpful in reducing coke formation on the catalyst surface. In our previous study, a novel 4-channel structured $\alpha\text{-}Al_2O_3$ hollow fiber,[29] with a surface area to volume ratio as high as 3,000 m^2/m^3, was used as catalyst

support where small Ni nanoparticles were deposited by ALD, and exhibited an excellent performance in a DRM reaction.[30] To further enhance the catalytic performance of the nickel-based hollow fiber catalysts, the addition of CeO_2 onto ALD-prepared Ni/Al_2O_3 hollow fibers could be a promising strategy. In this work, Ni nanoparticles were deposited on the 4-channel α-Al_2O_3 hollow fibers by ALD and different amounts of CeO_2 were introduced to the catalyst. The catalysts were systematically characterized and the catalytic performance was studied at atmospheric pressure in a temperature range of 700-850 °C.

2. Experimental

2.1. Catalyst preparation

4-channel α-Al_2O_3 hollow fibers[29] were used as catalyst support. Ni nanoparticles were deposited on the hollow fibers by ALD using bis(cyclopentadienyl)nickel ($NiCp_2$, Alfa Aesar) and hydrogen as precursors at 300 °C in a viscous flow reactor, as described in our previous work.[30] The hollow fibers were hung in the ALD reactor and heated at 150 °C, with 6 mL/min N_2 flow, overnight to remove adsorbed moisture (pressure about 300 Pa). The $NiCp_2$ was heated at 85 °C to provide the precursor vapor and carried by 6 mL/min N_2 to dose into the reactor for 300 s. Then, 6 mL/min N_2 were used to flush the sample to remove the unreacted precursor and any byproducts for 600 s and, then, the system was evacuated by vacuum pump for 10 s. Pure H_2 was then used as a precursor to dose into the reactor for 300 s. The same procedures were conducted, including a N_2 purge for 600 s and vacuum evacuation for 10 s. During the dosing and flushing process, the pressures were about 320 Pa and 300 Pa, respectively; the pressure during evacuation was about 10 Pa. Five cycles of Ni ALD including pulse of $NiCp_2$ and H_2 were applied onto the hollow fibers, and the catalyst was labeled as Ni/Al_2O_3HF-ALD.

CeO_2 was introduced into the synthesized catalyst by an incipient wetness (IW) method, using $Ce(NO_3)_3 \cdot 6H_2O$ (cerium nitrate hexahydrate, Alfa Aesar, 99.99%) as a precursor. The synthesized Ni/Al_2O_3HF-ALD catalyst was added into an aqueous solution containing cerium nitrate hexahydrate (1.0 g hollow fiber sample with 1.5 mL solution) and dried at 100 °C, with continuous stirring, followed by calcination in air at 500 °C for 3 h. Different amounts of CeO_2 (with a molar ratio of Ce/Ni = 0.25, 0.42, and 0.75) were added onto the Ni/Al_2O_3HF-ALD sample, labeled as 0.25CeNi/Al_2O_3HF-ALD, 0.42CeNi/Al_2O_3HF-ALD, and 0.75CeNi/Al_2O_3HF-ALD, respectively.

For ease of characterization, ALD-synthesized Ni catalysts on α-Al_2O_3 nanoparticles (Alfa Aser, 99+%, 80 nm, US3008) were prepared to investigate the promotional effect of CeO_2. The Ni ALD process was carried out in a fluidized bed reactor, as reported in our previous work.[30] The α-Al_2O_3 nanoparticles were put in the fluidized ALD reactor and heated at 150 °C, with 10 mL/min N_2 flow overnight, to remove adsorbed moisture. Then similar procedures, including a precursor dose for 180 s, N_2 purge for 300 s, and evacuation for 10 s, were conducted for five cycles to prepare the catalyst, which was labeled as Ni/Al_2O_3NP-ALD.

For comparison, Ni nanoparticles on α-Al_2O_3 nanoparticles were synthesized by an incipient wetness method, labeled as Ni/α-Al_2O_3NP-IW. The same α-Al_2O_3 nanoparticles were impregnated in an aqueous solution (1.0 g α-Al_2O_3 nanoparticles sample with 0.7 mL solution) containing nickel nitrate hexahydrate ($Ni(NO_3)_2 \cdot 6H_2O$, Alfa Aesar, 98.0%), dried at 100 °C, followed by calcination in air at 500 °C for 3 h. In addition, CeO_2 was introduced onto the

Ni/Al_2O_3NP-ALD and Ni/Al_2O_3NP-IW samples with a Ce/Ni molar ratio of 0.42 (the optimal ratio for hollow fiber catalysts that we found in this study), using the same incipient wetness method (1.0 g α-Al_2O_3 nanoparticle sample with 0.7 mL solution) as above, labeled as $CeNi/Al_2O_3$NP-ALD and $CeNi/Al_2O_3$NP-IW, respectively.

2.2. Dry reforming of methane

Catalysts were loaded in a vertical quartz tube reactor (inner diameter=10 mm) for DRM reactions and inert quartz wool was employed to support the catalysts. The hollow fiber catalysts were cut into short pieces (~0.8 cm long) and packed parallel in the reactor tube; for the nanoparticle catalysts, the catalysts (without being diluted) were put on the quartz wool in the reactor. A tube furnace was employed to heat up the reactor. Gas flow rates were monitored and controlled by MKS® mass flow controllers and the reaction temperatures were measured using a K-type thermocouple inside the reactor. An online gas chromatograph (SRI 8610C), equipped with a 6-foot Hayesep D column, a 6-foot molecular sieve 13X column, and a thermal conductivity detector (TCD), was employed to analyze the reaction products.

Before the DRM reaction, the catalysts were reduced at 700 °C, for 1 h, in 100 mL/min 20vol.%H_2/80vol.%Ar. After reduction, the flow of H_2 was stopped and the reactor temperature was elevated to 850 °C with an increase rate of 10 °C/min. In a typical DRM reaction, a gas mixture of CH_4 (99.9%) and CO_2 (99%) (CH_4/CO_2 = 1 molar ratio, with a total flow rate of 60 mL/min) was introduced into the reactor. The reaction was first carried out at 850 °C for a certain time and, then, the reaction temperature was decreased to 800 °C. After running the reaction for a certain time of stream, the catalysts were regenerated and applied for the DRM

reaction again. The regeneration process consisted of oxidation at 700 °C for 1 h in 100 mL/min 20vol.%O_2/80vol.%Ar, returning to an ambient temperature in 60 mL/min Ar and reduction in 100 mL/min 20vol.%H_2/80vol.%Ar for 1 h at 700 °C.

2.3. Catalyst characterization

The contents of Ni and Ce on the catalysts were investigated by inductively coupled plasma-optical emission spectroscopy (ICP-OES), using a 2000D Perkin Elmer, and the samples were dissolved by a mixture of H_2O_2, H_2SO_4, and H_3PO_4. The surface area of samples was tested using Brunner−Emmet−Teller (BET) measurements, with Quantachrome Autosorb-1. The morphology of supported Ni catalysts was observed by transmission electron microscopy (TEM), with a FEI Tecnai F20 TEM. X-ray diffraction spectra were collected using a Philips X-Pert Multi-purpose Diffractometer, with Cu Kα 1 radiation (λ=0.15416 nm). The samples were reduced at 700 °C in 100 mL/min 20vol.%H_2/80vol.%Ar flow for XRD test. X-ray photoelectron spectroscopy (XPS) spectra were recorded using a Kratos Axis 165 X-ray photoelectron spectrometer. A monochromatic Al Kα radiation (hν = 1486.6 eV) was used as the radiation source, and the takeoff angle was 0°. H_2-temperature programmed reduction (H_2-TPR) was conducted on a Micromeritics AutoChem Ⅱ 2920 instrument. A certain amount of catalyst powder (~ 150 mg) was placed in a U-shape quartz tube. The temperature program contained a preheat treatment at 500 °C in Ar flow, returning to ambient temperature in Ar flow and temperature ramping of 30-1,000 °C at a rate of 10 °C /min in 10vol.%H_2/90vol.% Ar flow. Sequential CH_4-TPSR (temperature-programmed surface reaction)/CO_2-TPO (temperature-programmed oxidation)/O_2-TPO was conducted using 200 mg catalyst in the same reactor as the dry reforming test. The procedures consisted of reduction in 20vol.%H_2/80vol.%Ar at 700 °C,

returning to ambient temperature, reaction in 30 mL/min 20vol.%CH_4/80vol.%Ar flow (200-900 °C, 10 °C/min), returning to ambient temperature, reaction in 30 mL/min 20vol.%CO_2/80vol.%Ar flow (200-900 °C, 10 °C/min), returning to ambient temperature and reaction in 30 mL/min 20vol.%O_2/80vol.%Ar flow (200-900 °C, 10 °C/min). The outlet gas was detected by mass spectrum (QMS200 Gas Analyzer, Stanford Research System). The valves of m/e at 2, 16, 28, 32, 40, and 44 were identified as H_2, CH_4, CO, O_2, Ar, and CO_2, respectively. O_2-TPO for spent catalysts was conducted using the same equipment. 30 mg spent nanoparticle catalysts were tested in the quartz tube from 100-850 °C, with a temperature ramping rate of 5 °C/min in 20 mL/min 10vol.%O_2/90vol.%Ar flow. The CO_2 signal with m/e=44 was plotted as a function of temperature and little change was observed for a signal with m/e=28 for CO. CO_2-TPD was conducted using the same instrument with ~100 mg catalyst powder in a quartz tube. The temperature program contained a preheat treatment at 500 °C in Ar flow, returning to ambient temperature in Ar flow, adsorption in 10vol.%CO_2/90vol.%Ar at ambient temperature, flush in Ar flow at 80 °C for 1 h, and temperature ramping of 80-800 °C at a rate of 10 °C /min in Ar flow. Scanning electron microscopy with energy dispersive spectroscopy (SEM-EDS, Philips MPD) was employed to study the carbon deposition of spent catalysts.

3. Results and Discussion

3.1. Characterization of fresh catalysts

Ni content was 0.11 wt. % for a Ni/Al_2O_3HF-ALD catalyst, 1.49 wt. % for Ni/Al_2O_3NP-ALD, and 1.50 wt. % for Ni/Al_2O_3NP-IW, based on ICP-OES analysis. From the BET test, the Ni/Al_2O_3NP-ALD had a surface area of about 11.2 m^2/g whereas, after CeO_2 introduction, the surface area changed to 10.7 m^2/g, which indicated that the introduction of CeO_2 had little effect

on the surface and porous structure of the support. In addition, XRD (in Figure S1) verified the peaks for Ni and CeO_2 of CeNi/Al_2O_3NP-ALD. TEM was employed on the Ni/Al_2O_3NP-ALD and Ni/Al_2O_3HF-ALD samples. As shown in Figure 1a, the black spots were deposited Ni nanoparticles; the Ni nanoparticles, with an average particle size of 3.1 ± 0.7 nm, were highly dispersed on the support. After CeO_2 was introduced onto the Ni/Al_2O_3NP-ALD sample, the average Ni particle size was 3.3 ± 1.0 nm (Figure 1b), therefore, the Ni nanoparticles prepared by ALD were stable enough to undergo the calcination process during the CeO_2 addition by the IW method. For Ni/Al_2O_3HF-ALD (Figure 1c), well dispersed nickel nanoparticles could be identified as the small white spots. By analyzing the recognizable spots, the average size of Ni deposited on HF was approximately 5.1 ± 1.6 nm.

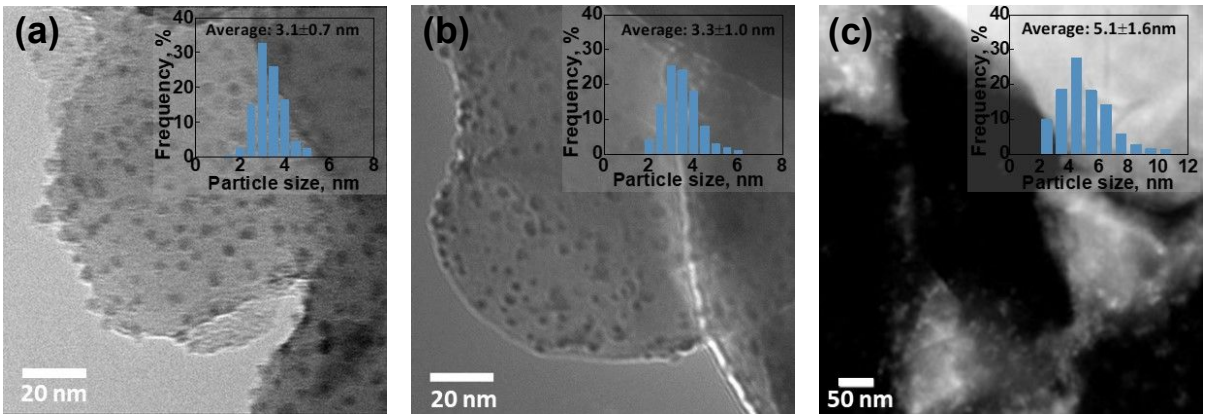

Figure 1. TEM images of (a) Ni/Al_2O_3NP-ALD, (b) CeNi/Al_2O_3NP-ALD, and STEM image of (c) Ni/Al_2O_3HF-ALD. The inset images show size distributions of Ni nanoparticles.

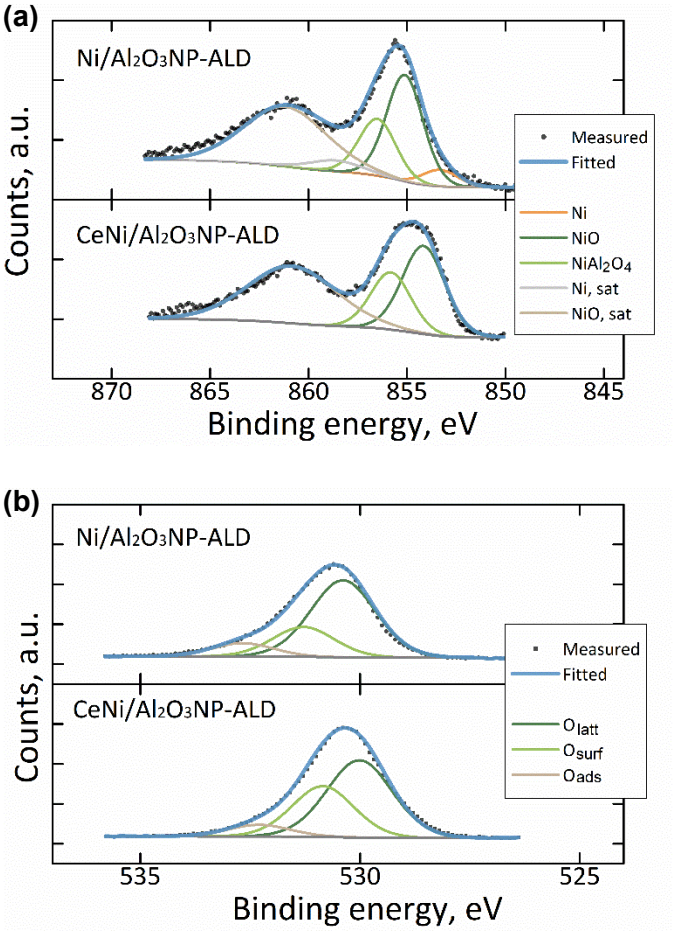

Figure 2. XPS core levels of Ni/Al_2O_3NP-ALD and $CeNi/Al_2O_3NP$-ALD: (a) Ni $2p_{3/2}$ and (b) O 1s.

High resolution XPS of Ni $2p_{3/2}$ and O 1s was conducted for Ni/Al_2O_3NP-ALD and $CeNi/Al_2O_3NP$-ALD to gain insight into the binding energy between Ni nanoparticles and the support. All XPS samples were calibrated with the C=C peak of the adventitious carbon peak at 284.5 eV in C1s (see Figure S2, Figure S3, and Table S1 for details). As shown in Figure 2a, in terms of Ni species, the peaks could be divided into metallic Ni, NiO, $NiAl_2O_4$, satellite Ni, and satellite NiO [31]. For Ni/Al_2O_3NP-ALD, the peak of metallic nickel was observed at 853.2 eV. The peak

of NiO at 855.2 eV was higher than that of the bulk NiO, as reported with a binding energy at approximately 854 eV,[32] which indicated that Ni (II) was in interaction with the Al_2O_3 support. The shake-up satellite peaks of nickel were at 858.8 eV for metallic Ni (0) and 861.2 eV for Ni (II), respectively. The peak at 856.4 eV was ascribed to the spinel $NiAl_2O_4$ component. In our previous study of ALD-synthesized Ni on γ-Al_2O_3 support, spinel nickel aluminate was convinced to be generated during the ALD process.[12] Similar to other ALD processes,[33, 34] the Ni-ALD process would be rationally postulated to be initiated when the O-H bond on Al_2O_3 surface was replaced by O-Ni bond,[35] forming Al-O-Ni-Cp or Al-O-Ni-C_xH_y and, in the following step, H_2 would participate in surface reaction and remove the -Cp or -C_xH_y species. Considering the strength of the Al-O-Ni bond, it would be possible that a part of the nickel might still bond with Al_2O_3 during the dose of hydrogen, to form thermal-stable $NiAl_2O_4$, which would be significant for catalytic performance including catalytic activity and thermal stability.

With the introduction of CeO_2 to Ni/Al_2O_3NP-ALD, the peak of Ni and Ni satellite disappeared because the metallic nickel was oxidized to NiO during the calcination process in air using the IW method. Obviously, the peak of NiO shifted to 854.3 eV, which was close to that of the bulk NiO [32], and the peak of $NiAl_2O_4$ shifted to 856.0 eV. The decrease in binding energy indicated that the interaction between NiO and Al_2O_3 was inhibited by the introduction of CeO_2, probably due to the diffusion of CeO_2 into the NiO-Al_2O_3 phase.[11, 26] For the DRM reaction, it was generally believed that metallic nickel was the active site for the reaction. For this work, NiO, with weakened metal-support interaction by the introduction of CeO_2, was supposedly more likely to be reduced to active metallic nickel nanoparticles for the catalytic reaction.

XPS of O 1s was conducted and deconvoluted to determine the chemical state of the oxygen species, as shown in Figure 2b. Three peaks were observed for both catalysts, O_{latt} at 530 eV for lattice oxygen in the metal oxide, O_{surf} at 531 eV for the surface oxygen, including defect oxide and adsorbed oxygen ions, and O_{ads} at 532 eV for the hydroxyl species or adsorbed water species.[36, 37] With the introduction of CeO_2, the percentage of O_{surf}, with higher mobility and activity,[38-40] increased from 23.2% to 32.5%. Due to the strong oxygen storage and release capacity of the Ce^{4+}/Ce^{3+} couple, oxygen defects were generated on the CeO_2 surface,[26, 37] which could enhance the adsorption and surface reaction, and further improve the catalytic activity of CO_2 and intermediate CH_x.

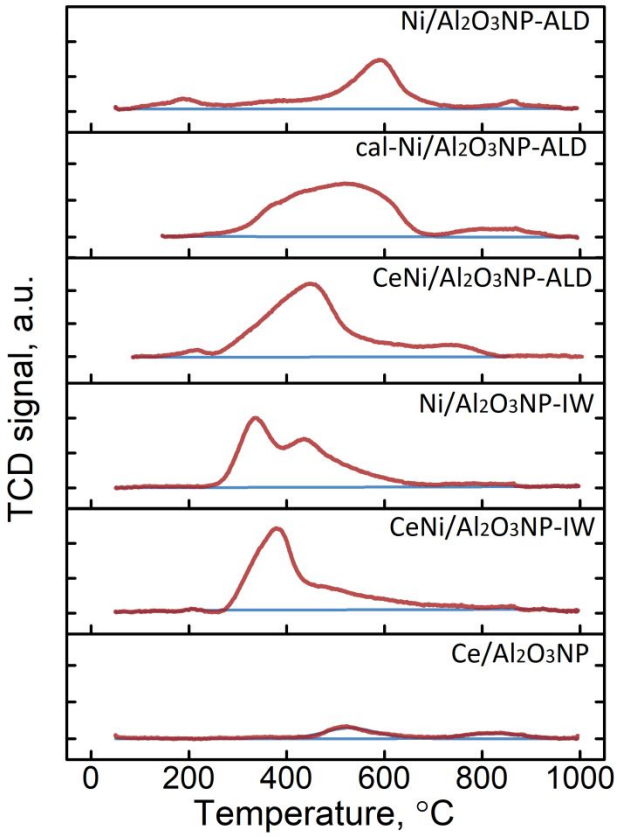

Figure 3. H_2-TPR profiles of Ni/Al_2O_3NP-ALD, cal-Ni/Al_2O_3NP-ALD, $CeNi/Al_2O_3NP$-ALD, Ni/Al_2O_3NP-IW, $CeNi/Al_2O_3NP$-IW, and Ce/Al_2O_3NP.

Temperature program reduction (H_2-TPR) was conducted to study the metal-support interaction of supported Ni catalysts, as shown in Figure 3 and Figure S4. As shown in Figure S4, the reduction peaks of the bulk NiO was located at 400 °C, denoted as α-NiO, and the bulk spinel $NiAl_2O_4$ were located at 835 °C, denoted as γ-NiO. The TPR profiles of catalysts in Figure 3 are definitely not the simple combination of NiO and $NiAl_2O_4$; the peaks with intermediate reduction temperature range (about 500-700 °C) should be NiO-Al_2O_3 phase with different extent of diffusion (or called non-stoichiometric $NiAl_xO_y$), denoted as β-NiO in literatures.[11, 13, 27, 31, 41] In terms of CeO_2 in CeO_2/Al_2O_3, the peak at lower temperature was ascribed to the reduction of reducible surface capping oxygen of CeO_2, whereas the peak at high temperature was ascribed to reduction Ce^{4+} to Ce^{3+} in bulk CeO_2.[28] For the Ni/Al_2O_3NP-ALD sample in Figure 3, the peaks are mainly NiO-Al_2O_3 (β-NiO) at 590 °C with small amount of NiO (α-NiO) and $NiAl_2O_4$ (γ-NiO), whereas only NiO (α-NiO) and NiO-Al_2O_3 (β-NiO) peaks were observed for Ni/Al_2O_3NP-IW. The existence of $NiAl_2O_4$ (γ-NiO) for Ni/Al_2O_3NP-ALD indicated that the NiO-Al_2O_3 interaction of the ALD-prepared catalyst was stronger than that of the IW-prepared catalyst, because of the surface reaction between the nickel precursor and Al_2O_3 support during the ALD process.[12] In addition, a small peak only observed for Ni/Al_2O_3NP-ALD at 200 °C might be the oxygen absorbed on the metallic nickel [18, 42] or amorphous surface of NiO.[14]

With regard to the Ni/Al_2O_3 system, the interaction between NiO and Al_2O_3 is the key for the stability of catalysts through the prevention of the sintering of Ni nanoparticles.[13] In this study, the reaction temperature of 850 °C had already exceeded the reduction temperature of $NiAl_2O_4$, as demonstrated in the H_2-TPR results. This meant that $NiAl_2O_4$ was not a completely stable

phase and could be gradually reduced in the reductive atmosphere of H_2 and CO, the main products of the DRM reaction. The further reduction of $NiAl_2O_4$, during the reaction, would generate more nickel for the reaction.[17, 19, 20] In terms of the high stability of the $NiAl_2O_4$, there should still be an appreciable amount of $NiAl_2O_4$ remaining under the DRM condition. Although $NiAl_2O_4$ could help stabilize the metallic nickel and maintain a high thermal stability of the catalysts, with respect to the utilization of Ni, excessive $NiAl_2O_4$ would lead to an inevitable latent activity loss,[15] since $NiAl_2O_4$ was inactive for the reaction. It is important to tune the reducibility of $NiAl_2O_4$ to retain balanced amounts of Ni and $NiAl_2O_4$, which are responsible for high catalytic activity and high thermal stability, respectively.

As CeO_2 was introduced to Ni/Al_2O_3NP-ALD, the peaks for NiO, NiO-Al_2O_3, and $NiAl_2O_4$ were shifted to lower temperatures, as compared to those of the calcined Ni/Al_2O_3NP-ALD in the same condition (noted as cal-Ni/Al_2O_3NP-ALD), indicating that NiO was easier to reduce due to the effect of CeO_2. Especially, the peak for $NiAl_2O_4$ for CeO_2 promoted Ni/Al_2O_3NP-ALD was shifted to a lower temperature (below 810 °C) and, therefore, the $NiAl_2O_4$ could be easier to reduce with the effect of CeO_2, which was also confirmed by TPR of the CeO_2-added $NiAl_2O_4$ (in Figure S4). The improved reducibility of oxidized nickel species might be ascribed to the fact that the introduced CeO_2 might replace Ni^{2+} in the NiO-Al_2O_3 or drive the Ni^{2+} away from the NiO-Al_2O_3 or $NiAl_2O_4$ phase. As mentioned earlier, the DRM reaction temperature in this study was above the reduction temperature of $NiAl_2O_4$ and, therefore, a higher reducibility of oxidized nickel tuned by CeO_2 was very important for catalytic performance. The higher reducibility of $NiAl_2O_4$ could form an additional amount of active metallic Ni during reaction and, to a greater extent, further activate the catalyst for DRM.

To gain a deeper insight into the effect of CeO_2 on catalyst active sites for dry reforming of methane, sequential CH_4-TPSR/CO_2-TPO/O_2-TPO was conducted to exhibit adsorption, surface reaction, and desorption[11, 14, 43, 44] at catalytic sites for CH_4 and CO_2 separately. The results are shown in Figure 4. In respect of CH_4-TPSR, the CH_4 reaction mainly consisted of adsorption of CH_4 on the metallic nickel, dissociation of the C-H bond,[45] and formation of hydrogen and residual CH_x species, which still adsorbed on the Ni surface and would terminate surface reactions.[44] The CH_4 peak for CeNi/Al_2O_3NP-ALD was observed at 597 ˚C, as compared to 609 ˚C of Ni/Al_2O_3-ALD. A similar peak shift was also observed for Ni/Al_2O_3NP-IW and CeNi/Al_2O_3NP-IW, which indicated that CeO_2 could enhance the activity of Ni in CH_4 dissociative adsorption.[22, 28] In terms of CH_4 consumption, the peak area of CeNi/Al_2O_3-ALD was larger than that of Ni/Al_2O_3-ALD. In contrast, there was no difference in the CH_4 peak area for IW-synthesized catalysts, with or without CeO_2. The extra CH_4 consumption could be ascribed to the fact that CeO_2 tuned the reducibility of the $NiAl_2O_4$ phase in the ALD-synthesized catalyst and led to the formation of more Ni(0) after reduction, whereas there was only a negligible amount of reducible $NiAl_2O_4$ for the IW-synthesized catalyst.

For the following CO_2-TPO, the CO_2 reaction consisted of adsorption of CO_2, dissociation of CO_2, and formation of active oxygen O* and its further reaction with residual CH_x species, to generate CO and H_2. Notably, the more CH_4 consumption for CeNi/Al_2O_3NP-ALD than Ni/Al_2O_3NP-ALD would result in more carbon residence. Larger CO_2 consumption was observed for CeNi/Al_2O_3NP-ALD than that for Ni/Al_2O_3NP-ALD, which indicated that CeO_2 significantly enhanced the CO_2 surface reaction. In addition, there were additional CO_2

consumption peaks, and a CO generation peak appeared at 650 °C for the CeO_2 promoted Ni/Al_2O_3 catalyst. However, there was only one peak at around 800 °C for the as-prepared Ni/Al_2O_3 catalyst, indicating that dissociative adsorption of CO_2 took place with the assistance of CeO_2 in a more efficient pathway than the pristine catalyst. As reported in the literature, CeO_2 has a strong oxygen storage capacity (OSC), due to the Ce^{4+}/Ce^{3+} couple[26, 31, 41] and, therefore, it would enhance dissociative adsorption of CO_2 and formation of O*, which is a key intimidation for residual gasification.[45] The enhanced CO_2 adsorption on $CeNi/Al_2O_3$NP-ALD was also observed by CO_2-TPD, as shown in Figure S5; the addition of CeO_2 may improve the basic sites[44, 46] of the catalysts for CO_2 adsorption.

In addition, the following O_2-TPO exhibited that there was still some carbon residue left in all samples, even after CO_2-TPO. From the area of O_2 consumption and CO_2 production in the O_2-TPO, conclusions could be made that there was less CH_x residue left from CH_4 dissociation because the CeO_2 could strongly enhance the CO_2 activity to gasificate the CH_x residence. In this way, the CeO_2-promoted catalyst would have a better coke inhibition because of higher activity in the CO_2 reaction for gasification of coke, or coke precursor, which was consistent with our experimental results.

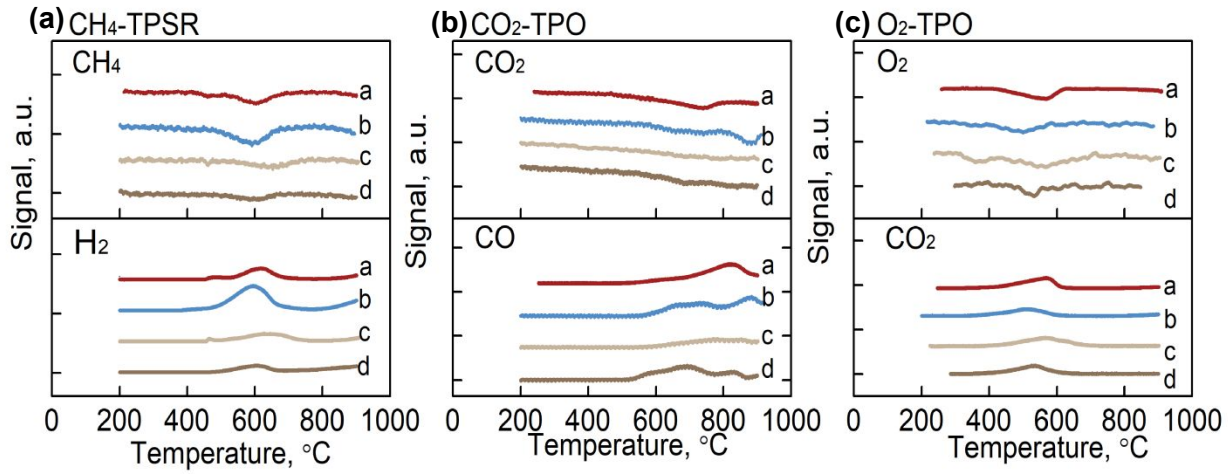

Figure 4. Sequential CH_4-TPSR/CO_2-TPO/O_2-TPO profiles of nickel-based nanoparticle catalysts after reduction: a. Ni/Al_2O_3NP-ALD, b. CeNi/Al_2O_3NP-ALD, c. Ni/Al_2O_3NP-IW, and d. CeNi/Al_2O_3NP-IW.

3.2. Dry reforming of methane

The ALD-prepared Ni/Al_2O_3HF-ALD catalysts, with and without CeO_2 (with Ce/Ni molar ratio of 0, 0.25, 0.42, and 0.75), were employed to catalyze the DRM reaction. The results are shown in Figure 5 and Figure S6, with equilibrium conversion data in Figure S7. The DRM reactions were carried out at 850 °C, first for 72 h and, then, the reaction temperatures were decreased to 800 °C for 72 h (Figure 5a and Figure S6a). All catalysts showed increasing performances in the first 30 h, which could have been due to the fact that Ni(II) in $NiAl_2O_4$ was gradually reduced by generated H_2 and CO at a high reaction temperature during the DRM reaction,[12] and then showed a stabilized performance at 850 °C, after a certain length of reaction time. All CeO_2-promoted catalysts had a better performance than that of the pristine catalyst, while the 0.42CeNi/Al_2O_3HF-ALD catalyst showed the best performance with a methane reforming rate as high as 2,410 $Lh^{-1}g_{Ni}^{-1}$ at 850 °C. The introduction of CeO_2 onto the catalyst significantly

increased the catalyst performance, which could be attributed to the fact that CeO_2 could modify the interaction between NiO and Al_2O_3,[11] increase the reducibility of the $NiAl_2O_4$ spinal to metallic Ni and, thus, activate the catalyst during the reaction. With the further increase of the CeO_2 contents, the catalyst activity decreased, probably because the excessive CeO_2 would cover some of the Ni reactive sites. After the reaction temperatures were set to 800 °C, the 0.42CeNi/Al_2O_3HF-ALD catalyst still showed the best performance among all of the hollow fiber-supported catalysts.

To check the capability of catalyst regeneration, all catalysts were regenerated via a procedure of oxidation, followed by reduction after 144 h of DRM reactions (72 h at 850 °C and 72 h at 800 °C). The regenerated catalysts were applied for a DRM reaction again. As shown in Figure 5b and Figure S6b, after regeneration, all catalysts in the second cycle showed good activity. Here, one cycle means a DRM reaction at different temperatures without regeneration. Among all of the catalysts, the 0.42CeNi/Al_2O_3HF-ALD catalyst still showed the highest activity with a methane reforming rate of 2,460 $Lh^{-1}g_{Ni}^{-1}$. It should be noted that the regenerated CeNi/Al_2O_3HF-ALD catalysts in the 2nd cycle test achieved a higher activity without activation; the 0.42CeNi/Al_2O_3HF-ALD catalyst showed 86.7% conversion in the 1st cycle and 88.4% conversion in the 2nd cycle, probably due to the removal of carbon deposition during the regeneration process. In contrast, the regenerated Ni/Al_2O_3HF-ALD catalyst had an activity loss (71.8% conversion in the 1st cycle and 69.5% conversion in the 2nd cycle), which might indicate a possible sintering took place for pristine catalyst and the CeO_2 could help stabilize the Ni nanoparticles. Therefore, in this study, 0.42:1 was the optimal Ce/Ni molar ratio to enhance the catalyst activity for the ALD-synthesized Ni on hollow fiber catalysts.

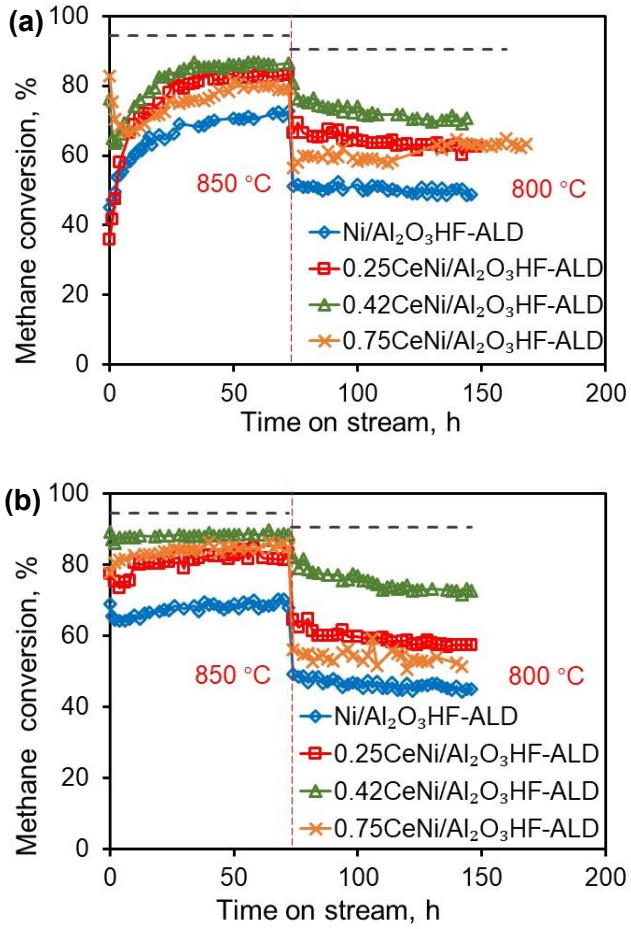

Figure 5. Methane conversion of (a) the first cycle and (b) the second cycle of dry reforming of methane reactions catalyzed by Ni/Al_2O_3HF-ALD, $0.25CeNi/Al_2O_3HF$-ALD, $0.42CeNi/Al_2O_3HF$-ALD, and $0.75CeNi/Al_2O_3HF$-ALD. Reaction conditions: catalyst loading of 0.6 g, 0.11 wt.% Ni, reactant composition of CH_4/CO_2=50/50 vol. %, and total flow rate of 60 mL/min. Note: Dash lines are equilibrium methane conversion.

To further investigate the effects of CeO_2 introduction on the catalytic performance of the Ni/α-Al_2O_3 system, both Ni/Al_2O_3NP-ALD and $CeNi/Al_2O_3NP$-ALD, with higher Ni loadings than the hollow fiber samples, were employed to catalyze the DRM reaction, because a higher Ni loading allowed smaller activity changes. As shown in Figure 6, both catalysts demonstrated a

slow activation process at the initial stage of the reaction at 850 °C. This activation was due to the gradual reduction of the relatively stable $NiAl_2O_4$ species that formed during the ALD process in a reductive atmosphere (i.e., H_2 and CO generated from DRM) at 850 °C, as reported in our previous work.[12] Obviously, a longer activation time was needed for the $CeNi/Al_2O_3$NP-ALD catalyst to reach a steady performance. The longer activation time was simply not due to a slower activation rate, since similar activation rates were observed for both catalysts at the initial stage (8.1 $Lh^{-1}g_{Ni}^{-1}$/h for $CeNi/Al_2O_3$NP-ALD and 8.6 $Lh^{-1}g_{Ni}^{-1}$/h for Ni/Al_2O_3NP-ALD). In fact, the longer activation time was due to the fact that the amount of reducible $NiAl_2O_4$ species increased with changes in reaction conditions, because CeO_2 weakened the NiO-Al_2O_3 interaction and, thus, increased the reducibility of the $NiAl_2O_4$ species to metallic Ni. Eventually, the Ce Ni/Al_2O_3NP-ALD catalyst reached a reaction rate of 1330 $Lh^{-1}g_{Ni}^{-1}$, which was about 17% higher than that of Ni/Al_2O_3 (1,100 $Lh^{-1}g_{Ni}^{-1}$) at 850 °C, and also higher than those of IW-prepared catalysts (in Figure S8). The recyclability of the Al_2O_3 nanoparticle supported catalysts (Ni/Al_2O_3NP-ALD and $CeNi/Al_2O_3$NP-ALD) is shown in Figure S9, and their catalytic performances of the 2nd cycle were similar to those of the 1st cycle test. The performance of our catalysts is superior, compared to those of other reported catalysts, as listed in Table 1. The high activity should be ascribed to the highly dispersed Ni nanoparticles prepared by the ALD synthesis method and the promoting effect of CeO_2. Notably, the reaction rate increased from 780 to 1330 $Lh^{-1}g_{Ni}^{-1}$ during the activation process for Ce Ni/Al_2O_3NP-ALD catalyst, which indicates the CeO_2 promoting effect could better utilize the nickel by improving the reducibility of $NiAl_2O_4$.

When the temperature was set lower than 800 °C, both catalysts went through a relatively steady stage with a very slow deactivation. The CeNi/Al_2O_3NP-ALD catalyst showed a much slower deactivation rate, even after a longer reaction time at 850 °C. For instance, the CeNi/Al_2O_3NP-ALD had a deactivation rate of -1.1 $Lh^{-1}g_{Ni}^{-1}/h$, only 40% of the -2.8 $Lh^{-1}g_{Ni}^{-1}/h$ for Ni/Al_2O_3NP-ALD at 800 °C. The ratio of deactivation rate of Ce-promoted/as-prepared catalysts further decreased to 35% at 750 °C and, then, to 29% at 700 °C. This could be ascribed to the fact that CeO_2 could inhibit coke formation. From the CH_4-TPSR/CO_2-TPO/O_2-TPO results, the mobile oxygen of CeO_2 could enhance the dissociative adsorption and surface reaction of CO_2 with adsorbed CH_x and, therefore, would reduce coke formation during the dry reforming of methane.

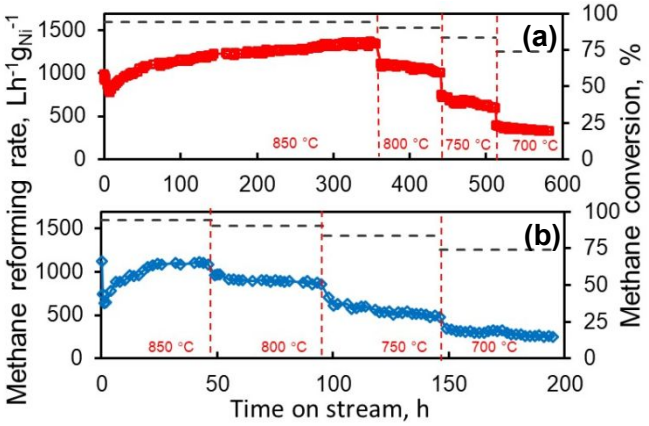

Figure 6. Methane reforming rate and conversion of dry reforming of methane reactions catalyzed by (a) CeNi/Al_2O_3NP-ALD and (b) Ni/Al_2O_3NP-ALD. Reaction conditions: catalyst loading of 0.070 g, 1.49 wt.% Ni, reactant composition of CH_4/CO_2=50/50 vol. %, total flow rate of 60 mL/min. Note: Dash lines are equilibrium methane conversion.

Table1. Comparison of methane reforming rates of dry reforming of methane reaction catalyzed by different catalysts in this work and in the literature.

Catalyst	Methane reforming rate ($Lh^{-1}g_{Ni}^{-1}$)				Reference
	850 °C	800 °C	750 °C	700 °C	
CeNi/Al_2O_3HF-ALD	2410	2000	-	-	This work
CeNi/Al_2O_3NP-ALD	1330	1050	680	380	This work
NiCe/Al_2O_3	-	290	250	225	[16]
Ni/CeO_2-γ-Al_2O_3	-	550	430	310	[20]
Ni/CeO_2-Al_2O_3	270	250	200	160	[41]
Ni-Zr/MCM-41	-	580	560	510	[47]
Ni/$Ce_{0.75}Zr_{0.25}O_2$	270	240	190	150	[48]
Ni-CaO-ZrO_2	430	-	350	-	[49]
Ni/SBA-15	225	210	170	150	[50]

3.3. Characterization of spent catalysts

To further understand the promotional effects of CeO_2 for the ALD Ni catalysts, the Ni/Al_2O_3NP-ALD and CeNi/Al_2O_3NP-ALD catalysts after 72 h of DRM at 850 °C were characterized using XPS (Figure 7 and Figure S3). As shown in Figure 7, the peaks for Ni, NiO, and $NiAl_2O_4$ were observed for both catalysts. The NiO was probably due to the inevitable oxidation by oxygen when the catalyst was exposed to air. The existence of $NiAl_2O_4$ in both catalysts demonstrated that certain amounts of $NiAl_2O_4$ still remained unreduced, even after reduction before the DRM reaction, and in a highly reductive environment during the DRM reaction (i.e., H_2 and CO reductive atmosphere at 850 °C for 72 h). Here, the ratio of

$NiAl_2O_4$/(Ni+NiO) was taken as a reference of the spinel degree. The ratio of $NiAl_2O_4$/(Ni+NiO) was 0.33 for Ni/Al_2O_3NP-ALD, and 0.37 for CeNi/Al_2O_3NP-ALD, because the heat treatment during the addition of CeO_2 by the IW method should favor the spinel $NiAl_2O_4$ formation. After reaction, the ratio was 0.31 for spent Ni/Al_2O_3NP-ALD and 0.20 for spent CeNi/Al_2O_3NP-ALD, which verified that more $NiAl_2O_4$ became reducible under the same condition. This was consistent with the characterization of fresh catalysts and our DRM reaction results.

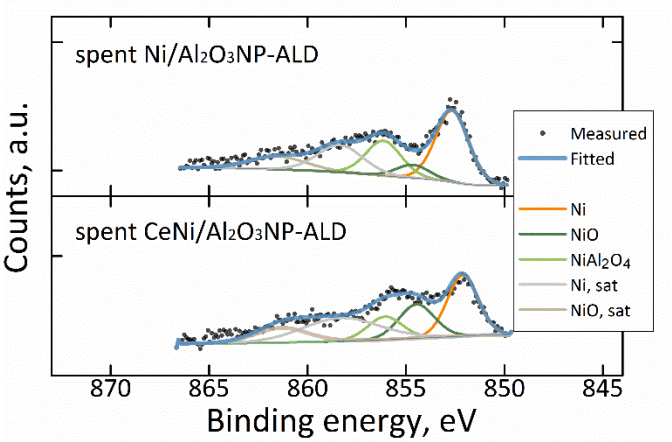

Figure 7. XPS core levels of Ni $2p_{3/2}$ of spent Ni/Al_2O_3NP-ALD and spent CeNi/Al_2O_3NP-ALD, after DRM at 850 °C for 72 h.

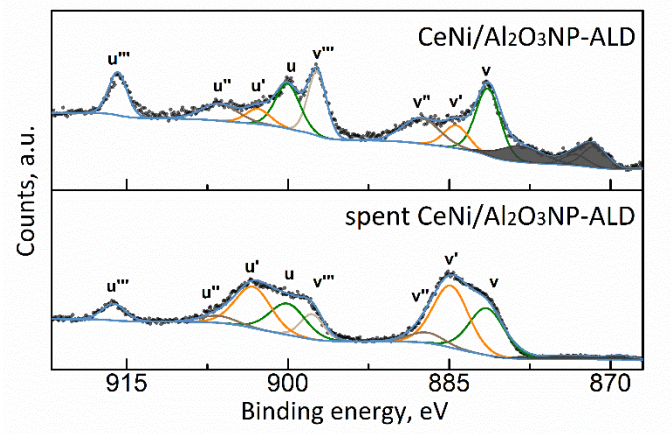

Figure 8. XPS core levels of Ce3d of fresh CeNi/Al_2O_3NP-ALD and spent CeNi/Al_2O_3NP-ALD, after DRM at 850 °C for 72 h.

In order to investigate the chemical state of the Ce element during the reaction, Ce3d was fitted using the fresh CeNi/Al_2O_3NP-ALD and spent CeNi/Al_2O_3NP-ALD samples, as show in Figure 8. Due to the overlapping of Ni2p and Ce3d, the peaks for Ni2p (the dark grey part) were deducted by applying the signal ratio of Ni2p3/2 to Ni2p1/2 at 2:1. Ascribed to the transition to different final states,[51] the Ce^{4+} peaks could be fitted into spin orbit photoelectron Ce 3d5/2 peaks, including v at 881.4 eV, v" at 887.6 eV, v"' at 897.4 eV, and corresponding Ce 3d3/2 peaks, including u at 900.0 eV, u" at 906.3 eV, u"' at 915.8 eV,[31, 51] whereas Ce^{3+} had a Ce 3d5/2 peak v' at 884.6 eV and its corresponding Ce 3d3/2 peaks u' at 903 eV.[31, 51] Herein, for better quantification of the chemical valence change of Ce, the u"'% of the Ce 3d was applied to evaluate the content of Ce(IV), and the (v'+u')% was applied to evaluate the content of Ce(III).[31] The u"'% was 11.0% for the fresh CeNi/Al_2O_3NP-ALD, which was close to the 13.4% for CeO_2 as reported;[31] and the u"'% was 4.8% for the spent CeNi/Al_2O_3NP-ALD. The lower Ce^{4+} content for spent CeNi/Al_2O_3NP-ALD was ascribed to the reduction of Ce^{4+} to Ce^{3+} during the reduction pretreatment and during the DRM reaction. In addition, the (u'+v')% from 12.8% for fresh CeNi/Al_2O_3NP-ALD, compared to 45.7% for spent CeNi/Al_2O_3NP-ALD, exhibited that there was a significant amount of Ce^{3+} generated from Ce^{4+} during the reaction.

The reduction of Ce(IV) to Ce(III) during the reaction probably led to the formation of much more thermally favored $CeAlO_3$, as compared to Ce_2O_3.[43, 52, 53] $CeAlO_3$ was reported to be highly stable for the CeO_2/Al_2O_3 system under a reductive atmosphere at high temperature.[43] Therefore, the Ce^{3+} ion reduced from CeO_2 might react with Al_2O_3 to form $CeAlO_3$ (R1), or probably dope into $NiAl_2O_4$ to form $CeAlO_3$ (R2), and drive Ni^{2+} from the $NiAl_2O_4$ to form NiO, which would

be quickly reduced to Ni. As shown in Figure S10, both assumed reactions should be thermodynamically favored under reaction conditions with the Gibbs free energy less than zero, whereas, without the assistance of CeO_2 or H_2, the direct decomposition of $NiAl_2O_4$ was impossible. To further verify the possibility of $CeAlO_3$ formation, XRD was conducted on the CeO_2-added $NiAl_2O_4$ after reduction (similar as the reaction condition), as shown in Figure S11. The XRD result indicated that there was significant formation of $CeAlO_3$ instead of Ce_2O_3 after high temperature reduction. By forming stable $CeAlO_3$, NiO might be freed from NiO-Al_2O_3 or $NiAl_2O_4$, and then be reduced by H_2 with the assistance of Ce^{4+}/Ce^{3+}, which would explain the higher reducibility of $NiAl_2O_4$, tuned by CeO_2, and longer activation period during the reaction.

$$Ce_2O_3 + Al_2O_3 \rightarrow 2CeAlO_3 \quad (R1)$$

$$Ce_2O_3 + NiAl_2O_4 \rightarrow 2CeAlO_3 + NiO \quad (R2)$$

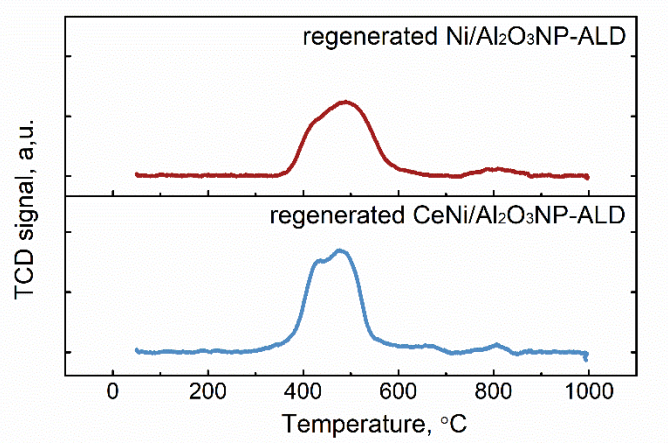

Figure 9. H_2-TPR profiles of regenerated Ni/Al_2O_3NP-ALD and CeNi/Al_2O_3NP-ALD (after the 1st cycle of dry reforming reaction, followed by oxidation at 700 °C in 100 mL/min 20vol.%O_2/ 80vol.%Ar for 1hr).

In order the investigate the metal-support interaction of the catalysts after reaction and the recyclability of the catalysts, TPR was conducted on the regenerated Al_2O_3 NPs supported

catalysts (after the 1st cycle reaction followed by oxidation at 700 °C in 100 mL/min 20vol.%O_2/ 80vol.%Ar for 1hr). As shown in Figure 9, the predominant nickel oxide components are α-NiO without metal-support interaction (similar to bulk NiO) and β-NiO with slight NiO-Al_2O_3 interaction, and only a small amount of $NiAl_2O_4$ could be detected. By comparing the fresh (Figure 3) and regenerated (Figure 9) catalysts, we can draw the conclusion that most of $NiAl_2O_4$ (γ-NiO) have been reduced during the activation of the first cycle of DRM and the regenerated samples were easier to be reduced, which can explain that the regenerated catalyst (both hollow fiber and alumina nanoparticle supported catalysts) didn't undergo the gradual reduction of $NiAl_2O_4$ (activation process) and achieved the high activity directly. However, there was still part of $NiAl_2O_4$ remained at the interface, as verified by XPS analysis (Figure 7). In terms of the promoting effect of CeO_2, the reduction temperature for regenerated CeNi/Al_2O_3NP-ALD was significantly lower than that of regenerated Ni/Al_2O_3NP-ALD, and this means that the α-NiO (at 410 °C) was predominate for the regenerated CeNi/Al_2O_3NP-ALD catalyst, whereas the β-NiO (at 500 °C) was predominate for the regenerated Ni/Al_2O_3NP-ALD catalyst. In addition, more $NiAl_2O_4$ was detected in the regenerated Ni/Al_2O_3NP-ALD. It would be rational to postulate that the CeO_2 or $CeAlO_3$ can reduce the NiO-Al_2O_3 interaction and inhibit the formation of $NiAl_2O_4$ during the reaction.

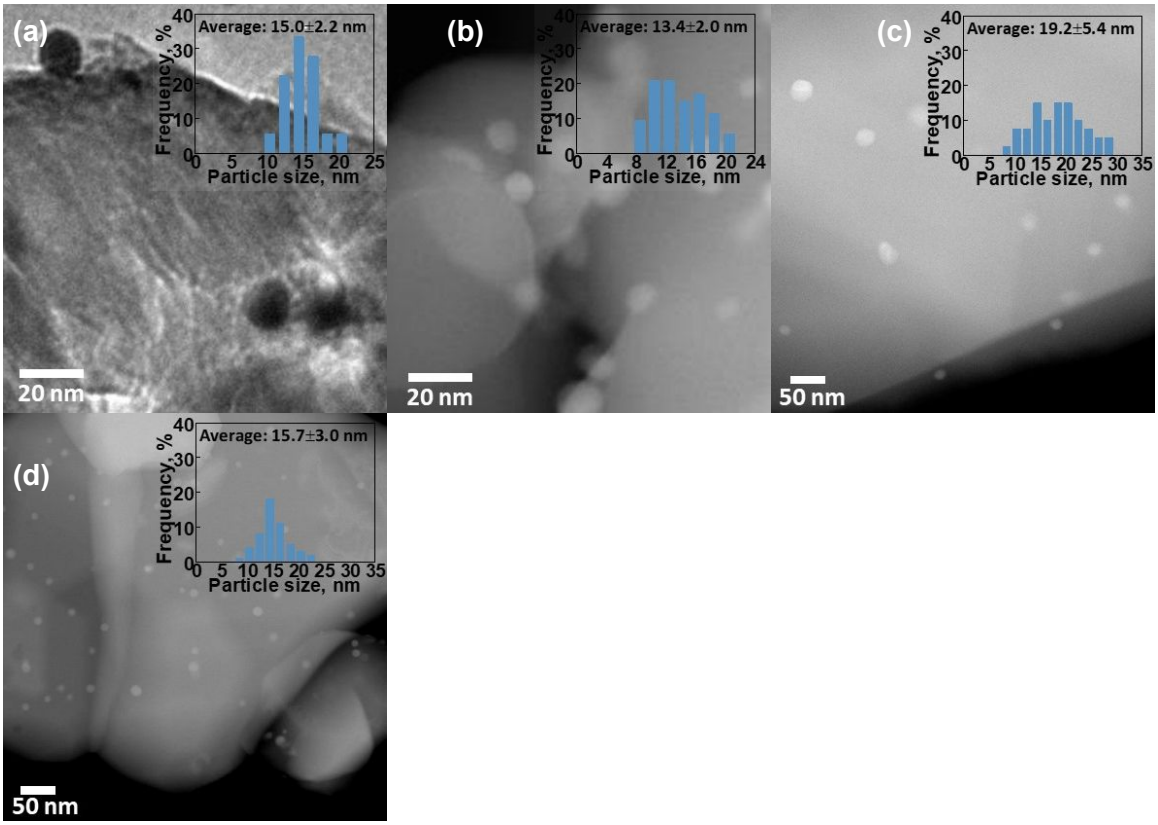

Figure 10. (a) TEM image of spent Ni/Al_2O_3NP-ALD and (b) STEM image of spent CeNi/Al_2O_3NP-ALD after DRM at 850 °C for 72 h; STEM images of (c) spent Ni/Al_2O_3HF-ALD and (d) spent CeNi/Al_2O_3HF-ALD after two cycles of DRM reaction (Note: 72 h at 850 °C and 72 h at 800 °C for one cycle). The inset images show size distributions of Ni nanoparticles.

Morphology of spent nanoparticle and hollow fiber supported catalysts are shown in Figure 10, with the inhibiting effect of the introduction of CeO_2 on the sintering of nickel nanoparticles. The average size of Ni was at 15.0 ± 2.2 nm for spent Ni/Al_2O_3NP-ALD (Figure 10a), and 13.4 ± 2.0 nm for spent CeNi/Al_2O_3NP-ALD (Figure 10b) after 72 h of DRM reaction at 850 °C. Similar results were also observed for spent hollow fiber catalysts. Here, the spent Ni/Al_2O_3HF-ALD and spent CeNi/Al_2O_3HF-ALD (after two cycles of DRM reaction) had an average particle size of

19.2 ± 5.4 nm and 15.7± 3.0 nm, respectively. The inhibiting effect on sintering could be ascribed to the interaction of CeO_2 and NiO-Al_2O_3 during the reaction.

Coking is another cause for deactivation of Ni-based catalysts from a DRM reaction. We believe that the addition of CeO_2, not only improved the reducibility of $NiAl_2O_4$ to catalytically active Ni, but also inhibited coke formation. To verify this, nickel-based hollow fiber catalysts, with and without CeO_2, were analyzed after two cycles of reaction (one cycle of reaction consisted of 72 h of DRM reaction at 850 °C and 72 h of reaction at 800 °C), using a scanning electron microscope (SEM) and an energy dispersive spectrometer (EDS). As shown in Figure S12, there was less carbon deposition on the surfaces of CeO_2 promoted catalysts. The average surface carbon content of Ni/Al_2O_3HF-ALD, 0.25CeNi/Al_2O_3HF-ALD, 0.42CeNi/Al_2O_3HF-ALD, and 0.75CeNi/Al_2O_3HF-ALD was 7.4 wt.%, 3.6 wt.%, 3.3wt.%, and 2.5 wt.%, respectively, indicating that CeO_2 did inhibit coke formation. The coke inhibiting capacity of CeO_2 could be ascribed to the enhanced dissociative adsorption of CO_2 on CeO_2, as discussed in TPSR.

O_2-TPO was conducted to further study of carbon deposition on spent Ni/Al_2O_3NP-ALD and CeNi/Al_2O_3NP-ALD, after dry reforming of methane at 850 °C for 72 h, as shown in in Figure 11. Peaks that appeared below 300 °C for both catalysts could be related to carbidic carbon (C_α) on nickel.[38, 54, 55] The higher temperature of the carbon species could be ascribed to amorphous carbon (C_β),[38, 54, 55] 605 °C for Ni/Al_2O_3NP-ALD, and 565 °C for CeNi/Al_2O_3NP-ALD, respectively. The lower oxidation temperature for CeO_2 promoted catalysts could be due to the oxygen storage and release capacity of CeO_2, which was similar to the CO_2-TPO process discussed earlier. In addition, the notable peak at 660 °C for Ni/Al_2O_3NP-ALD could be ascribed to graphitic carbon (C_γ),[38, 54-56] whereas no C_γ peak was detected for CeNi/Al_2O_3NP-ALD. This

meant that CeO_2 could have a strong inhibiting effect on coke formation during reaction, especially the graphitic carbon.[43]

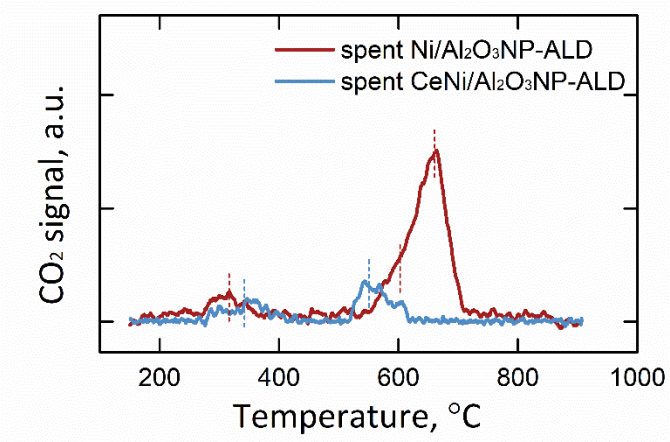

Figure 11. TPO profiles of spent Ni/Al_2O_3NP-ALD, $CeNi/Al_2O_3$NP-ALD after 72 h of DRM at 850 °C.

4. Conclusion

In this work, CeO_2 was introduced onto ALD-synthesized nickel nanoparticles on 4-channel structured α-Al_2O_3 hollow fibers and α-Al_2O_3 nanoparticles using an incipient wetness method. Various characterizations (i.e., XRD, XPS, TRP, TPSR, SEM-EDS, and TPO) indicated that the introduced CeO_2 could weakened the NiO-Al_2O_3 interaction and free NiO from NiO-Al_2O_3 or $NiAl_2O_4$ by the formation of stable $CeAlO_3$ under a reductive atmosphere, thereby improving the reducibility of NiO species. With the introduction of CeO_2, more $NiAl_2O_4$ could be gradually reduced to the metallic nickel by the reaction product (i.e., H_2 and CO) during the DRM reaction at 850 ˚C. In addition, the incompletely-reduced $NiAl_2O_4$ could stabilize the metallic nickel nanoparticles. Remarkably, $CeNi/Al_2O_3$NP-ALD had an activation phenomena lasting 360 h, which was 7.5 times longer that of Ni/Al_2O_3NP-ALD. The optimal $CeNi/Al_2O_3$HF-ALD catalyst, with Ce/Ni=0.42, reached a methane reforming rate of 2,410 $Lh^{-1}g_{Ni}^{-1}$ at 850 °C. This was 19%

higher than that of the Ni/Al_2O_3HF, and the catalyst exhibited an excellent performance after regeneration. In addition, the strong oxygen storage and release properties of CeO_2 improved the CO_2 dissociative adsorption reaction, and led to less carbon deposition and, thereby, higher stability for nickel-based catalysts.

Acknowledgements

This work was supported by the U.S. Department of Energy (Contract Number DE-FE0029760). We thank DOE/NETL Project Manager, Bruce W. Lani, for his assistance and support.

References:

1. W. Zhou, J.-G. Chen, K.-G. Fang and Y.-H. Sun, *Fuel. Process. Technol*, 2006, **87**, 609-616.
2. D. Tristantini, S. Lögdberg, B. Gevert, Ø. Borg and A. Holmen, *Fuel. Process. Technol*, 2007, **88**, 643-649.
3. H. Wang and E. Ruckenstein, *Appl. Catal. A: Gen*, 2000, **204**, 143-152.
4. A. M. O'Connor, Y. Schuurman, J. R. Ross and C. Mirodatos, *Catal. Today*, 2006, **115**, 191-198.
5. P. G. Schulz, M. G. Gonzalez, C. E. Quincoces and C. E. Gigola, *Ind. Eng. Chem. Res*, 2005, **44**, 9020-9029.
6. C. Carrara, J. Munera, E. A. Lombardo and L. M. Cornaglia, *Top. Catal*, 2008, **51**, 98-106.
7. M. M. Barroso-Quiroga and A. E. Castro-Luna, *Int. J. Hydrog. Energy*, 2010, **35**, 6052-6056.
8. Z. Hou, P. Chen, H. Fang, X. Zheng and T. Yashima, *Int. J. Hydrog. Energy*, 2006, **31**, 555-561.
9. F. Pompeo, N. N. Nichio, M. G. González and M. Montes, *Catal. Today*, 2005, **107**, 856-862.
10. G. Li, L. Hu and J. M. Hill, *Appl. Catal. A: Gen*, 2006, **301**, 16-24.

11. J. Zhang, H. Xu, X. Jin, Q. Ge and W. Li, *Appl. Catal. A: Gen*, 2005, **290**, 87-96.
12. Z. Shang, S. Li, L. Li, G. Liu and X. Liang, *Appl. Catal. B: Environ*, 2017, **201**, 302-309.
13. L. Zhou, Y. Guo, Q. Zhang, M. Yagi, J. Hatakeyama, H. Li, J. Chen, M. Sakurai and H. Kameyama, *Appl. Catal. A: Gen*, 2008, **347**, 200-207.
14. Z. Qin, J. Ren, M. Miao, Z. Li, J. Lin and K. Xie, *Appl. Catal. B: Environ*, 2015, **164**, 18-30.
15. L. Zhou, L. Li, N. Wei, J. Li and J. M. Basset, *ChemCatChem*, 2015, **7**, 2508-2516.
16. L. Zhang, X. Wang, C. Chen, X. Zou, X. Shang, W. Ding and X. Lu, *RSC Adv*, 2017, **7**, 33143-33154.
17. P. Littlewood, S. Liu, E. Weitz, T. J. Marks and P. C. Stair, *Catal. Today*, 2019.
18. C. Jiménez-González, Z. Boukha, B. de Rivas, J. J. Delgado, M. Á. Cauqui, J. R. González-Velasco, J. I. Gutiérrez-Ortiz and R. López-Fonseca, *Appl. Catal. A: Gen*, 2013, **466**, 9-20.
19. Y.-g. Chen and J. Ren, *Catalysis Letters*, 1994, **29**, 39-48.
20. S. Therdthianwong, N. Summaprasit, N. Junpanichravee and A. Therdthianwong, *Asian J. Energy Environ*, 2002, **3**, 1-25.
21. S. Sengupta, K. Ray and G. Deo, *Int. J. Hydrog. Energy*, 2014, **39**, 11462-11472.
22. S. Therdthianwong, A. Therdthianwong, C. Siangchin and S. Yongprapat, *Int. J. Hydrog. Energy*, 2008, **33**, 991-999.
23. N. Laosiripojana, W. Sutthisripok and S. Assabumrungrat, *Chem. Eng. J*, 2005, **112**, 13-22.
24. J. Zhu, X. Peng, L. Yao, J. Shen, D. Tong and C. Hu, *Int. J. Hydrog. Energy*, 2011, **36**, 7094-7104.
25. M. Goula, A. Lemonidou and A. Efstathiou, *J. Catal*, 1996, **161**, 626-640.
26. H. Liu, X. Zou, X. Wang, X. Lu and W. Ding, *J. Nat. Gas. Chem*, 2012, **21**, 703-707.
27. W. Zheng, J. Zhang, Q. Ge, H. Xu and W. Li, *Appl. Catal. B: Environ*, 2008, **80**, 98-105.
28. S. Damyanova, B. Pawelec, R. Palcheva, Y. Karakirova, M. C. Sanchez, G. Tyuliev, E. Gaigneaux and J. Fierro, *Appl. Catal. B: Environ*, 2018, **225**, 340-353.
29. Z. Shi, Y. Zhang, C. Cai, C. Zhang and X. Gu, *Ceram. Int*, 2015, **41**, 1333-1339.
30. Z. Shang, S. Li, Q. Wang, X. Gu and X. Liang, *AIChE J*, 2018, **64**, 2625-2631.

31. K. Kamonsuangkasem, S. Therdthianwong, A. Therdthianwong and N. Thammajak, *Appl. Catal. B: Environ*, 2017, **218**, 650-663.
32. M. A. Peck and M. A. Langell, *Chem. Mater*, 2012, **24**, 4483-4490.
33. W. Kessels, H. Knoops, S. Dielissen, A. Mackus and M. Van de Sanden, *Appl. Phys. Lett*, 2009, **95**, 013114.
34. W. Setthapun, W. D. Williams, S. M. Kim, H. Feng, J. W. Elam, F. A. Rabuffetti, K. R. Poeppelmeier, P. C. Stair, E. A. Stach and F. H. Ribeiro, *J. Phys. Chem. C*, 2010, **114**, 9758-9771.
35. T. D. Gould, A. M. Lubers, B. T. Neltner, J. V. Carrier, A. W. Weimer, J. L. Falconer and J. W. Medlin, *J. Catal*, 2013, **303**, 9-15.
36. S. Chen, L. Zeng, H. Tian, X. Li and J. Gong, *ACS Catal*, 2017, **7**, 3548-3559.
37. Y. Liu, Y. Wu, Z. Akhtamberdinova, X. Chen, G. Jiang and D. Liu, *ChemCatChem*, 2018, **10**, 4689-4698.
38. C. Tang, L. Liping, L. Zhang, L. Tan and L. Dong, *Kinet. Catal*, 2017, **58**, 800-808.
39. S. Damyanova, B. Pawelec, K. Arishtirova, M. M. Huerta and J. Fierro, *Appl. Catal. B: Environ*, 2009, **89**, 149-159.
40. Z. Li and K. Sibudjing, *ChemCatChem*, 2018, **10**, 2994-3001.
41. I. Luisetto, S. Tuti, C. Battocchio, S. L. Mastro and A. Sodo, *Appl. Catal. A: Gen*, 2015, **500**, 12-22.
42. R. K. Singha, S. Das, M. Pandey, S. Kumar, R. Bal and A. Bordoloi, *Catal Sci Technol*, 2016, **6**, 7122-7136.
43. W. Chen, G. Zhao, Q. Xue, L. Chen and Y. Lu, *Appl. Catal. B: Environ*, 2013, **136**, 260-268.
44. M. Zhang, J. Zhang, Y. Wu, J. Pan, Q. Zhang, Y. Tan and Y. Han, *Appl. Catal. B: Environ*, 2019, **244**, 427-437.
45. C. Papadopoulou, H. Matralis and X. Verykios, in *Catalysis for alternative energy generation*, Springer, 2012, pp. 57-127.
46. H. Liu, D. Wierzbicki, R. Debek, M. Motak, T. Grzybek, P. Da Costa and M. E. Galvez, *Fuel*, 2016, **182**, 8-16.
47. D. Liu, X. Y. Quek, W. N. E. Cheo, R. Lau, A. Borgna and Y. Yang, *J. Catal*, 2009, **266**, 380-390.

48. J. Chen, Q. Wu, J. Zhang and J. Zhang, *Fuel*, 2008, **87**, 2901-2907.
49. Q. Chen, J. Zhang, B. Pan, W. Kong, Y. Chen, W. Zhang and Y. Sun, *Chem. Eng. J*, 2017, **320**, 63-73.
50. M. Zhang, J. Shengfu, H. Linhua, Y. Fengxiang, L. Chengyue and L. Hui, *Chinese Journal of Catalysis*, 2006, **27**, 777-781.
51. G. Pantaleo, V. La Parola, F. Deganello, R. Singha, R. Bal and A. Venezia, *Appl. Catal. B: Environ*, 2016, **189**, 233-241.
52. S. Damyanova, C. Perez, M. Schmal and J. M. Bueno, *Appl. Catal. A: Gen*, 2002, **234**, 271-282.
53. J. Shyu, W. Weber and H. Gandhi, *J. Phys. Chem*, 1988, **92**, 4964-4970.
54. L. Li, S. He, Y. Song, J. Zhao, W. Ji and C.-T. Au, *J. Catal*, 2012, **288**, 54-64.
55. L. Chen, Y. Lu, Q. Hong, J. Lin and F. Dautzenberg, *Appl. Catal. A: Gen*, 2005, **292**, 295-304.
56. H. Düdder, K. Kähler, B. Krause, K. Mette, S. Kühl, M. Behrens, V. Scherer and M. Muhler, *Catal Sci Technol*, 2014, **4**, 3317-3328.

Graphical Abstract